JOURNAL OF COMPUTATIONAL PHYSICS 54, 425–456 (1984)

Turbulent Combustion in Open and Closed Vessels*

JAMES SETHIAN

Department of Mathematics and Lawrence Berkeley Laboratory, University of California, Berkeley, California 94720

Received February 23, 1983; revised July 6, 1983

We present a numerical technique to approximate the solution of a simplified model of turbulent combustion. The method, which is particularly suited for flows at high Reynolds number, uses random vortex element techniques coupled to a flame propagation algorithm based on Huyghens' principle. We use this technique to analyze combustion in open and closed vessels. In the first experiment, we model a flame propagating in a swirling, viscous flow inside a closed square. Our results show the growth and development of counterrotating turbulent eddies and their effect on the flame. In the second experiment, we model turbulent combustion within a channel, in which flow enters through a slit at one end. Results detail the effects of exothermicity and viscosity on the speed and shape of the burning front.

I. INTRODUCTION

One problem in the study of internal combustion engines is to analyze the effect of turbulence on the propagation of a flame. The more reactants reached by the flame, the more energy released and the less unburnt fuel expelled at the end of a stroke. At high Reynolds numbers, turbulent eddies and recirculation zones form that affect the position of the flame and the distribution of unburnt fuel available for combustion. In this paper, we present a numerical technique to approximate the solution of a simplified model of turbulent combustion. We use this technique to analyze combustion in open and closed vessels. In the first experiment, we model a flame propagating in a swirling, viscous flow inside a closed square. Our results show the growth and development of counterrotating turbulent eddies and their effect on the flame. In the second experiment, we model turbulent combustion within a channel, in which flow enters through a slit at one end. Our results detail the effects of exothermicity and viscosity on the speed and shape of the burning front.

Most partial differential equation models of turbulent flow are based on a formulation of the Navier–Stokes equations with respect to a mean state, together with a set of equations to include such components as turbulence velocity and length scales. These models are of varying degrees of sophistication and complexity, ranging

* The author is currently supported through a NSF Mathematical Sciences Postdoctoral Fellowship. This work was supported in part by the Director, Office of Basic Energy Sciences, Engineering, Mathematical and Geosciences Division of the U.S. Department of Energy under Contract DE.AC03-76SF00098.

0021-9991/84 $3.00

from zero-equation models ("mean-field closures") to higher-order stress-equation models. For an excellent overview of these models, see [18]. Equally complex models for turbulent flame propagation can be formulated, containing such effects as turbulent mixing, flame speed dependence on curvature, and flame wrinking. For a discussion of the theory of turbulent flows with premixed reactants, see [3]. Numerical approximations of these models usually consist of finite difference formulations of the appropriate equations. Although such techniques work well in many cases, the need for a fine grid in the boundary layer where sharp gradients exist and the intrinsic smoothing and numerical viscosity associated with finite differences place a computational upper bound on the size of the Reynolds number that can be effectively modeled.

The random vortex method, introduced in [7], is specifically designed to deal with these problems. It is an approximation to the equations of viscous, incompressible flow at high Reynolds number that avoids the introduction of mean states and turbulence closure relations. It is important to point out that in our study we shall confine ourselves to two-dimensional flows, and this in fact constitutes a significant closure assumption that restricts our ability to study such three-dimensional effects as turbulent mixing. However, this is a limitation imposed by the vortex method described below, and does not apply to more general three-dimensional vortex methods, currently an area of active research.

The flow is represented by a collection of vortex "blobs" that yield an associated velocity field. Viscous diffusion is simulated by a random walk imposed on the vortex motion. Normal boundary conditions are met through the addition of a potential flow solution, and tangential boundary conditions are satisfied by a vorticity creation algorithm (vortex sheets). By avoiding the averaging and smoothing associated with finite difference calculations, this technique allows us to follow the development of large-scale coherent turbulent structures within the flow. Of course, we do not gain something for nothing; our solution has become a probabilistic one in which the exact location of any particular vortex element has little meaning. This, however, is no different from what one expects for high Reynolds number flow; no two physical experiments will produce the same exact results (see [15]). What we can hope to see, and indeed do, is the large-scale structure of the flow. The use of vortices to help identify coherent turbulent structures is physically reasonable, as pointed out in [19], and this technique has been applied successfully to flow past a cylinder [5], blood flow through heart valves [16], and turbulent mixing layers [1]; theoretical investigations on questions of convergence and accuracy of vortex methods have been provided in [2, 11, 12]. A review of vortex methods may be found in [14].

To describe combustion within the flow, we use the thin flame model for infinitely fast kinetics, commonly used in the analysis of premixed turbulent combustion (see [3]). This assumes an infinitely thin flame front, in which pressure fluctuations are neglected, the Mach number is assumed small, and combustion is characterized by a single-step irreversible chemical reaction taking place at a constant rate. A standard numerical approximation for such a model is to represent the flame front by a set of marker particles that move according to the equations of motion of flame

propagation. At each time step, interpolation through these markers provides an approximation to the position of the front. Because of the difficulty involved in accurately determining normals by this technique, the numerical approximation to the propagating front usually becomes unstable and develops oscillations. Furthermore, it has been shown [21] that the propagating front can develop cusps, similar to shocks, where the front is no longer differentiable and hence the normal direction is not defined. An alternate technique, introduced in [9], avoids these difficulties and capitalizes on the geometric nature of flame propagation described in [21]. A grid is imposed on the combustion domain and each cell is assigned a number corresponding to the amount of burnt fluid in that cell. At each time step, the position of the flame front can be reconstructed from these volume fractions.

The above random vortex method and flame algorithm were first applied together to model turbulent combustion over a backwards-facing step [10]. In modeling our problem of combustion inside vessels, we have made numerous improvements in these techniques. We use second-order time integration to advance the positions of the vortex elements, and show that such accuracy is desirable for our calculation. A fast Poisson solver is used to produce the potential flow needed to satisfy normal boundary conditions. We present an amended version of the flame algorithm that removes a bias discovered in the original scheme towards propagation in a particular direction. The calculation presented in [10] "smears" the boundary between the burnt and unburnt regions; we modify the flame algorithm and the hydrodynamic calculation so that the front remains sharp. Finally, we present a technique to determine the exact location of the flame in each cell, as seen by the flame propagation algorithm. In the case where the flame front acts as a line source of specific volume, this allows us to devise, with the help of a fast Poisson solver, an accurate direct technique of determining the velocity field produced by expansion along the flame front. This is in constrast to previous algorithms that make use of volume source elements placed in the center of each cell undergoing combustion, regardless of the location of the flame in that cell.

Although our model of turbulent combustion is an admittedly simple one, we believe that it can serve adequately in situations where one is interested in the interaction between high Reynolds number hydrodynamics and the speed and shape of the burning front. The results of our numerical experiments with the above algorithms show the effects of exothermicity and viscosity on the rate of combustion. We show that exothermic effects along the front increase the speed at which the flame travels through the domain, decreasing the amount of time required for the fluid within the vessel to become completely burnt. We show that viscous effects, on the other hand, both retard and accelerate flame advancement; although the turbulent eddies produced by the no-slip condition inhibit burning in corners and near solid walls, they also wrinkle the flame, increasing the surface area available for combustion.

Section II details the assumptions and idealizations in our combustion model, and the mathematical formulation of the equations of motion. In Section III, we describe our numerical technique for modeling hydrodynamics, and apply it to a swirling fluid

impulsively started in a closed rectangle. In Section IV, we present the numerical scheme for following flame propagation, and use the combined algorithm to ignite our swirling flow. Finally, in Section V we present our technique for handling volume expansion along the front, and used this to model flame development in a channel.

II. The Combustion Model

A. *The Model*

We consider two-dimensional, viscous flow inside a given region. On solid walls, we require that the normal and tangential velocities be zero. We make the following assumptions:

(1) The fluid is a premixed fuel in which each particle can exist in one of two states, burnt and unburnt. When the temperature of an unburnt particle become sufficiently high, it undergoes an instantaneous change in volume due to heating and becomes burnt. The ratio of the density of a burnt particle to an unburnt particle depends on the mixture under study and is a prescribed constant. Thus, we regard the interface between the burnt and unburnt regions as an infinitely thin flame front, acting as a source of specific volume.

(2) The front propagates at a fixed speed in a direction normal to itself into the unburnt fluid. The lower the ignition temperature, the faster the flame propagates.

(3) Compressibility effects can be ignored, and sound waves travel infinitely fast; this balances pressure forces.

In our model, the fluid motion affects the position of the flame and the exothermic expansion along the front influences the fluid velocity. As an illustration of this process, consider flow in a channel. Suppose we ignite this fluid near the inlet, i.e., raise the temperature beyond the ignition point. As surrounding particles are ignited, their resulting change in volume pushes the fluid. This exothermic velocity field, added to the underlying fluid flow, carries the fluid, together with the flame front, down the channel.

In this model, we ignore variations in the flame propagation speed due to chemical kinetics, and disregard three-dimensional effects such as vortex stretching.

B. *Equations of Motion*

Let $\vec{u} = (u, v)$ be the velocity of the fluid at a point (x, y). With the assumption of an infinitely thin reaction zone, we view the flame front as a curve γ separating the burnt fluid from the unburnt fluid, where $\gamma(s, t)$ parameterizes by s the position of the flame front at time t. Thus, for each s, $\gamma(s, t)$ yields the coordinates (X_F, Y_F) of a fluid particle that is "on fire" at time t. Let R be the Reynolds number and k the prescribed flame propagation speed.

The fluid motion must satisfy the momentum equation for viscous flow (see [13]), namely,

$$\frac{D\vec{u}}{Dt} = \frac{1}{R}\nabla^2\vec{u} - \frac{\nabla\vec{P}}{\rho} \tag{2.1}$$

where D/Dt is the total derivative, $\vec{P} = \vec{P}(x, y)$ is the pressure, $\rho = \rho(x, y)$ is the density, ∇ is the gradient, and ∇^2 is the two-dimensional Laplacian. We restrict ρ to two possible values: ρ_u in the unburnt fluid and ρ_b in the burnt fluid. The boundary conditions for viscous flow are that $\vec{u} = 0$ on solid walls. The flow is incompressible on both sides of the flame front, hence $\nabla \cdot \vec{u} = 0$ in both the burnt and unburnt regions. However, along the front, where the fluid undergoes a volume expansions as it burns, the divergence is necessarily non-zero.

We may derive an expression for the effect of this volume expansion on the fluid velocity by using the conservation of mass. Since (ρu) must be continuous across the front,

$$\rho_u \bar{u}_{nu} = \rho_b \bar{u}_{nb} \tag{2.2}$$

where $\bar{u}_{nu}$ and $\bar{u}_{nb}$ are the velocities of the fluid normal to the front on the unburnt and burnt sides, respectively. The overbar denotes velocities taken relative to the moving front. Let u_{nu} and u_{nb} be the normal velocities on the unburnt and burnt sides, and let S be the speed of the front, all taken in a fixed frame. Then,

$$\rho_u(u_{nu} - S) = \rho_b(u_{nb} - S). \tag{2.3}$$

Solving for $(u_{nu} - u_{nb})$, we have

$$(u_{nu} - u_{nb}) = 2 \left\{\frac{\rho_u - \rho_b}{\rho_u + \rho_b}\right\} \left\{S - \left(\frac{u_{nb} + u_{nu}}{2}\right)\right\}. \tag{2.4}$$

The prescribed speed of propagation k plus the average of the normal velocities from the burnt and unburnt sides equals the observed speed, as seen from the fixed frame, thus across the flame front is a jump in normal velocity of strength

$$(u_{nu} - u_{nb}) = 2 \left\{\frac{\rho_u - \rho_b}{\rho_u + \rho_b}\right\} k. \tag{2.5}$$

To describe the motion of the flame front itself, we note that, as seen from a fixed reference frame, the front is both carried by the flow and advanced normal to itself by the burning process. As a point (X_F, Y_F) on the flame front, the normal vector of unit length pointing toward the unburnt fluid is

$$\left(\frac{1}{((X_F)_s^2 + (Y_F)_s^2)^{1/2}}\right) ((Y_F)_s, -(X_F)_s) \tag{2.6}$$

where the front is parameterized in such a way that the burnt region is on the left as we go along the front in the direction of increasing s. Thus, the motion of the front can be described by the system of partial differential equations

$$\frac{\partial X_F}{\partial t} = k(Y_F)_s \left(\frac{1}{((X_F)_s^2 + (Y_F)_s^2)^{1/2}}\right) + u(X_F, Y_F) \tag{2.7}$$

$$\frac{\partial Y_F}{\partial t} = -k(X_F)_s \left(\frac{1}{((X_F)_s^2 + (Y_F)_s^2)^{1/2}}\right) + v(X_F, Y_F). \tag{2.8}$$

Equations (2.1)–(2.8) characterize our model of flame propagation as a time-dependent free boundary value problem.

III. Hydrodynamics

In this section we describe our numerical technique for approximating the solution to the hydrodynamic component of our combustion equations (2.1)–(2.8). We shall follow the motion of vorticity, where vorticity is represented by a large number of discrete vortex elements spread throughout the domain. At each time step we will reconstruct the velocity field from the updated positions of the vortex elements. We consider flow inside a closed rectangle D with boundary ∂D. Since the flow is assumed incompressible in both the burnt and unburnt regions, we cannot allow volume expansion along the front in a closed vessel. Thus $\rho_u = \rho_b$. This restriction removes the feedback mechanism through which the flame affects the fluid flow. In a later section, we will consider combustion in a partially open vessel and thus be able to include density variations.

We take the curl of Eq. (2.1) to obtain the vorticity transport equation (see [13])

$$\partial_t \xi + (\vec{u} \cdot \nabla)\xi = (1/R)\nabla^2 \xi \tag{3.1}$$

where the vorticity $\xi = \nabla x \vec{u}$. We have used the fact that, with density constant throughout D, $\nabla x(\nabla \vec{P}/\rho) = 0$. Thus the flow is incompressible throughout D.

Our technique will be to divide the domain into an interior region and a boundary layer. In both regions, we will use the technique of operating splitting to break the relevant equations into an advection equation plus a diffusion equation. The solution in the bouncary layer will then be matched to the one obtained in the interior to produce the full flow.

In the interior, we solve the full vorticity transport equation in two stages. We first update the vorticity with respect to the advection component by solving

$$\begin{aligned} \partial_t \xi &= -(\vec{u} \cdot \nabla)\xi \\ \nabla \cdot \vec{u} &= 0 \end{aligned} \tag{3.2}$$

together with the boundary condition $(\vec{u} \cdot \vec{n}) = 0$, where $\vec{n}$ is the unit vector normal to the boundary of the interior. We then update the vorticity with respect to the diffusion term by solving

$$\partial_t \xi = (1/R)\nabla^2 \xi. \tag{3.3}$$

Combining these two solutions will provide, to a first approximation, a solution to (3.1) in the interior.

In the boundary layer, we use the Prandtl approximation to the Navier–Stokes

equations. This is derived from the assumptions that (1) vorticity is mainly produced from large gradients of u in the y direction, hence $\xi = \partial v/\partial x - \partial u/\partial y \approx -\partial u/\partial y$, and (2) along the wall, the diffusion of vorticity is small compared to advection, hence $\partial_x^2 \xi = 0$. (Here, x and y are directions parallel and normal to the solid wall, respectively). As before, our solution is split into two stages. First, we update the vorticity with respect to the advection component by solving

$$\begin{aligned} \partial_t \xi &= -(\vec{u} \cdot \nabla)\xi \\ \partial_x u + \partial_y v &= 0. \end{aligned} \tag{3.4}$$

We assume that the u velocity infinitely far from the wall is given, and require that both the normal and the tangential components of the velocity be zero along the solid wall. Second, we update the vorticity with respect to the diffusion term $\partial_y^2 \xi$.

Finally, we shall need a matching technique to "glue" the boundary layer calculation to the interior calculation. The relevant equations in each region are shown in Fig. 1.

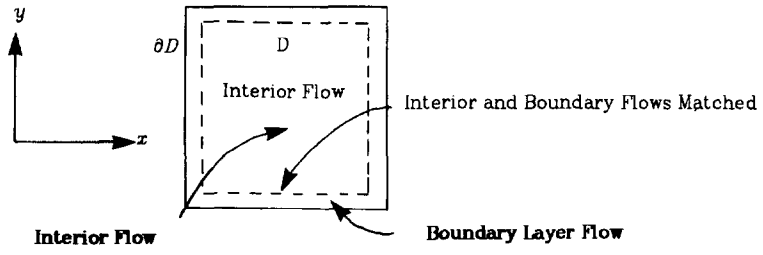

Navier-Stokes Equations Split Into:

1) Advection Equation:

$\partial_t \xi = -(\vec{u} \cdot \nabla)\xi$

$\xi = \nabla \times \vec{u}$

$\nabla \cdot \vec{u} = 0$

$\vec{u} \cdot \vec{n} = 0$ on interior boundary

$\xi(x, y, t=0)$ known

2) Diffusion Equation:

$\partial_t \xi = \frac{1}{R} \nabla^2 \xi$

Prandtl Boundary Layer Equations Split Into:

(Bottom Side)

1) Advection Equation:

$\partial_t \xi = -(\vec{u} \cdot \nabla)\xi$

$\xi = -\partial_y u$

$\nabla \cdot \vec{u} = 0$

$\vec{u} = 0$ on $\partial D\ (y=0)$

$u(x, y=\infty) = U_\infty(x)$

2) Diffusion Equation:

$\partial_t \xi = \frac{1}{R} \partial_y^2 \xi$

FIGURE 1

A. *Interior Flow: Advection*

We define a vortex blob of strength k_i located at $\bar{x}_i = (x_i, y_i)$ to be a concentration of vorticity occupying a small region and giving rise to a stream function

$$\psi_i(\bar{x}) = \left\{ \begin{array}{ll} \dfrac{k_i}{2\pi} \log r_i, & r_i > \sigma \\ \dfrac{k_i}{2\pi} \left(\dfrac{r_i}{\sigma} + \log \sigma - 1 \right), & 0 < r_i \leqslant \sigma \end{array} \right\}, \qquad r_i = |\bar{x} - \bar{x}_i| \tag{3.5}$$

where σ is the radius or "cutoff" of the blob. Associated with this stream function is a divergence-free velocity field $(u_{\text{vor},i}, v_{\text{vor},i}) = (-\psi_y, \psi_x)$; namely,

$$u_{\text{vor},i}(x, y) = \left\{ \begin{array}{ll} \dfrac{-k_i}{2\pi} \dfrac{y - y_i}{r_i^2}, & r_i \geqslant \sigma \\ \dfrac{-k_i}{2\pi} \dfrac{y - y_i}{\sigma r_i}, & 0 < r_i < \sigma \end{array} \right\}, \quad v_{\text{vor},i}(x, y) = \left\{ \begin{array}{ll} \dfrac{k_i}{2\pi} \dfrac{x - x_i}{r_i^2}, & r_i \geqslant \sigma \\ \dfrac{k_i}{2\pi} \dfrac{x - x_i}{\sigma r_i}, & 0 < r_i < \sigma \end{array} \right\} \tag{3.6}$$

This is the velocity field for a vortex blob introduced in [7]; it represents a smoothing of the stream function $\psi = \log r$ associated with a point vortex in such a way that the velocities remain bounded as one approaches the center of the blob. Since this center should not move under the above velocity field, we set $u = v = 0$ if $r_i = 0$. For details of this construction, see [7].

Our goal is to build the total vorticity distribution from a collection of vortex blobs. Assume that we are given an initial distribution of vorticity in D. We impose a grid on the domain, and place a vortex blob of strength k_i at the center of each cell of the grid, where k_i is the total amount of vorticity in that cell. Once this is done, we discard the grid; it plays no further role in our calculation. This collection of $i = 1,..., N$ vortex blobs produces a stream function ψ, where

$$\psi(\bar{x}) = \sum_{i=1}^{N} \psi_i(\bar{x}). \tag{3.7}$$

The velocity field induced by this stream function is just the superposition of the velocity fields produced by each individual blob, hence

$$u_{\text{vor}}(x, y) = \sum_{i=1}^{N} u_{\text{vor},i}, \qquad v_{\text{vor}}(x, y) = \sum_{i=1}^{N} v_{\text{vor},i}. \tag{3.8}$$

Our distribution of vortex blobs represents an approximation to the vorticity at the initial time. We can easily amend the above velocity field so that it satisfies the boundary conditions by finding a function φ_{pot} such that $\nabla^2 \varphi_{\text{pot}} = 0$ in D and $\partial \varphi_{\text{pot}} / \partial \vec{n} = -(\vec{u} \cdot \vec{n})$ on ∂D. This will provide us with a velocity field

$\nabla\varphi_{\text{pot}} = (u_{\text{pot}}, v_{\text{pot}})$ that is divergence-free, irrotational, and on the boundary exactly cancels the normal velocity component generated by the vortex blobs. Adding these two flows produces the required velocity field.

All that remains is to update the vorticity distribution in time. We must solve $\partial_t \xi = -(\vec{u} \cdot \nabla)\xi$, which is equivalent to the statement that vorticity is advected by its own velocity field. Thus, we move each vortex blob (x_i, y_i) as follows:

$$\frac{\partial x_i}{\partial t} = u_{\text{vor}}(x_i, y_i) + u_{\text{pot}}(x_i, y_i), \qquad \frac{\partial y_i}{\partial t} = v_{\text{vor}}(x_i, y_i) + v_{\text{pot}}(x_i, y_i). \tag{3.9}$$

Vorticity is conserved, since at any time we still have the same number of vortex blobs, each with its original strength. This is an attractive feature of vortex methods and is in direct contrast to finite difference methods that attempt to update the vorticity (or velocity) on a grid. In the latter technique, the error associated with the finite difference approximation can be significant and care must be taken so that vorticity is not "lost" on the grid. Regardless of the numerical technique chosen to solve the system of ordinary differential equations (3.9) and the potential flow problem, the errors arising from these approximations influence only the positioning of the vortex blobs, not the amount of vorticity.

Our calculation proceeded as follows. We imposed a square grid on the combustion domain. Given a collection of N blobs at time step n located at (x_i^n, y_i^n), $i = 1,..., N$, we calculated the normal component of the velocity field at those points of the grid lying on the boundary. We used the NCAR PDE Package [24] to solve the Neumann problem for a harmonic function in the domain whose normal derivative along the boundary exactly canceled the component produced by the blobs. Differentiation of this function on the grid and linear interpolation produced the velocity field $(u_{\text{pot}}, v_{\text{pot}})$ at any point. For the time integration (3.9) of the vortex blobs along their trajectories, Euler's method was used in [7] and [10]; we used Heun's method, namely,

$$x_{i_{\text{adv}}}^{n+1} = x_i^n + \frac{\Delta t}{2}\{(u_{\text{vor}}(x_i^n, y_i^n) + u_{\text{pot}}(x_i^n, y_i^n)) + (u_{\text{vor}}(x_i^*, y_i^*) + u_{\text{pot}}(x_i^*, y_i^*))\}$$

$$x_i^* = x_i^n + \Delta t[u_{\text{vor}}(x_i^n, y_i^n) + u_{\text{pot}}(x_i^n, y_i^n)] \tag{3.10}$$

$$y_{i_{\text{adv}}}^{n+1} = y_i^n + \frac{\Delta t}{2}\{(v_{\text{vor}}(x_i^n, y_i^n) + v_{\text{pot}}(x_i^n, y_i^n)) + (v_{\text{vor}}(x_i^*, y_i^*) + v_{\text{pot}}(x_i^*, y_i^*))\}$$

$$y_i^* = y_i^n + \Delta t[v_{\text{vor}}(x_i^n, y_i^n) + v_{\text{pot}}(x_i^n, y_i^n)] \tag{3.11}$$

where Δt is the time step and the subscript "adv" refers to the advection step. This technique is second-order accurate in time, as opposed to Euler's method, which is first-order accurate. Such accuracy is desirable, since as vortex blobs come close together, they spin around each other. Since a first-order scheme merely takes the tangent at a given point and constructs a straight line approximation to the trajectory, the effect will be to spread out the vortices. Obviously, this spreading is lessened by

the use of a higher-order scheme such as Heun's method. A multitime level scheme cannot be used, since the time integration is split between advection and a random walk component; thus one cannot "reach back" in time to construct a scheme for the purely advective motion.

As a test, we followed the motion of four vortices of equal strength and sign equally placed along a circle. It is easy to show that the vortices should revolve around the center. Using Euler's method to follow the vortex motion resulted in significant spreading of the vortices. For any choice of time step, the spreading was reduced by the use of Heun's method. Since Heun's method requires two evaluations of the velocity field per time step, this can prove expensive when using the direct $O(N^2)$ method of calculating vortex interaction; however, in any case a higher-order time scheme is clearly indicated. The development of fast techniques to evaluate vortex interactions (particle in cell, local corrections) will undoubtedly ease the cost of such methods, however, we shall, for this work, confine ourselves to the direct method.

B. *Interior Flow: Diffusion*

To update the vorticity distribution with respect to the diffusion term, we employ the technique of random walks. For the details of this construction, see [7]. Briefly, the technique is as follows.

Suppose one wished to solve the initial value problem on the real line

$$w_t(x, t) = (1/R)w_{xx}, \qquad w(x, 0) = \delta(x) \tag{3.12}$$

where $\delta(x)$ is the delta function. The solution of this one-dimensional diffusion equation is the Green's function $w(x, t) = (4\pi t/R)^{-1/2} \exp(-(x^2/(4t/R)))$, which corresponds to the probability density function associated with a Gaussian distribution with mean zero, variance $2t/R$. Thus, one can "solve" (3.12) by constructing this function as follows: At $t = 0$ place N particles, each with mass $1/N$, at the point $x = 0$. Allow each particle to undergo a random walk along the x axis, with the length of each step (either positive or negative) drawn from a Gaussian distribution with mean zero, variance $2\Delta t/R$, where $\Delta t = t/l$. After l steps, the position of each particle is just the sum of each of its displacements. For large N, the mass density distribution on the x axis has mean zero, variance $(l)(2\Delta t/R) = 2t/R$, and approximates $w(x, t)$. For more general initial data $w(x, 0) = f(x)$, the random walk solution can be constructed by distributing N particles uniformly along the x axis, where the ith particle, located at x_i, has mass $f(x_i)/N$. Then, after allowing each particle to undergo l random steps drawn from a Gaussian distribution with mean zero, variance $2\Delta t/R$, the mass distribution along the x axis at time $t = l\,\Delta t$ will approximate $w(x, t)$ for large N.

For our problem, we wish to model the diffusion of vorticity ($\partial_t \xi = (1/R)\,\nabla^2 \xi$) in two dimensions. At each time step, we have a collection of vortex blobs, each with mass corresponding to the vorticity density at a point. If we let each blob undergo a

random walk in both the x and y direction, the combined motion of the blobs will approximate the solution to the vorticity diffusion equation.

The combination of the solutions to the advection and diffusion equations produces our numerical algorithm for the solution of the Navier–Stokes equations in the interior: Given a collection of N vortex blobs at time $n\Delta t$, their position at time $(n+1)\Delta t$ is given by

$$x_i^{n+1} = x_{i_{\text{adv}}}^{n+1} + \eta_{i1} \tag{3.13}$$

$$y_i^{n+1} = y_{i_{\text{adv}}}^{n+1} + \eta_{i2} \tag{3.14}$$

where η_{i1} and η_{i2} are random variables drawn from the above Gaussian distribution.

Two comments should be made at this point. First, the above algorithm for advection and diffusion avoids the problem of grid-generated "artificial viscosity" that can plague finite difference schemes. In such techniques, the error associated with the finite difference approximation to the flow looks like a diffusion term, and this "numerical" viscosity, which is a function of grid size, can overshadow the effects of real physical viscosity at high Reynolds number and thus place an artificial upper bound on the size of the Reynolds number that can be effectively modeled. Such spatially generated "artificial" diffusion is avoided by the vortex blob/random walk algorithm. The error associated with moving the vortex blobs along their trajectories, while not yet completely analyzed from a theoretical point of view, is presumably not of this type, and is minimized through the use of a higher-order time integration scheme.

Second, it might seem that one must use a large number of particles to adequately model the diffusion. However, it is important to realize that we are modeling the diffusion of vorticity. In that case, the summation over the positions of the vortex elements to produce the velocity field at each time step corresponds to "integration," and thus produces a smoother function. Consequently, not that many particles are required for an adequate representation: numerical experiments have shown that around 100 particles produce a reasonable approximation.

C. *Boundary Layer: Advection + Diffusion*

As stated earlier, we assume that vorticity within the boundary layer is mainly produced from large gradients of u in the y direction ($\xi = -\partial u/\partial y$). This is because of the "no-slip" condition that requires the velocity to vanish at the boundary. Vorticity is produced as the moving fluid grabs onto the solid wall. The boundary layer acts as a transition zone from the still fluid at the wall to the high speed flow in the interior as vorticity created at the solid boundary diffuses into the main flow. This is in contrast to flow in the interior ($\xi = \nabla x \vec{u}$) where neither velocity component dominates the motion of vorticity. Consequently, it is inappropriate to use vortex blobs to discretize vorticity within the boundary layer, since each blob generates a radially symmetric rotation of fluid about its center. Instead, we make use of vortex "sheets," which are surfaces parallel to solid walls across which the tangential velocity changes abruptly. For a complete discussion of the use of vortex sheets in the boundary layer, see [8]. Briefly, the idea is as follows.

We begin by expressing u in terms of the vorticity. Integration of $\xi = -\partial_y u$ yields

$$u(x, y) = U_\infty + \int_y^\infty \xi(x, s)\, ds \tag{3.15}$$

where U_∞ is the velocity at infinity as viewed from the wall. Since the flow is incompressible, we may derive an expression for v in terms of u, namely,

$$v(x, y) = -\partial_x \int_0^y u(x, s)\, ds \tag{3.16}$$

where we have used the fact that $v(x, 0) = 0$. We define a vortex sheet of intensity ξ, length h, centered at (x_0, y_0) to be a line segment of length h, parallel to the x axis, such that $u(x, y_0^+) - u(x, y_0^-) = -\xi$.

Given a vorticity distribution within the boundary layer, that is, a collection of $i = 1,..., N$ vortex sheets centered at (x_i, y_i) with strengths ξ_i, we may approximate (3.15) by

$$u(x, y) = U_\infty + \sum_{y_i > y} \xi_i d_i \tag{3.17}$$

where the summation is performed over all sheets lying above y and $d_i = \max(0, 1 - |x - x_i|/h)$ represents the fraction of the ith sheet lying over the point (x, y). Thus, the u velocity at each point is determined only by those sheets lying in a narrow vertical strip above (x, y). Similarly, we may approximate (3.16) by

$$v(x, y) = \frac{-(I_+ - I_-)}{h} \tag{3.18}$$

where

$$I_\pm = U_\infty + \sum d_j^\pm y_j^*$$

$$d_j^\pm = \max(0, 1 - |x \pm h/2 + x_j|/h)$$

$$y_j^* = \min(y, y_j).$$

Formulae (3.17) and (3.18) provide us with the velocity field associated with our vorticity distribution. We first update the vorticity with respect to the advection equation $\partial_t \xi = -(\vec{u} \cdot \nabla)\xi$ by moving each sheet (x_i, y_i) according to (3.17) and (3.18). To update the vorticity with respect to the diffusion equation $\partial_t \xi = (1/R)\, \partial_y^2 \xi$, we again use a random walk solution and allow each sheet to undergo a jump in the y direction, either positive or negative, with the size of the jump drawn from a Gaussian distribution with mean zero, variance $2\Delta t/R$. Note that diffusion takes place

only in the direction normal to the wall. The position of the ith sheet at time $(n+1)\Delta t$ is given by

$$x_i^{n+1} = x_i^n + \frac{\Delta t}{2}\left[u_i(x_i, y_i) + u_i(x_i^*, y_i^*)\right] \tag{3.19}$$

$$y_i^{n+1} = y_i^n + \frac{\Delta t}{2}\left[v_i(x_i, y_i) + v_i(x_i^*, y_i^*)\right] + \eta_i \tag{3.20}$$

$$x_i^* = x_i^n + \Delta t\, u_i(x_i, y_i)^*$$

$$y_i^* = y_i^n + \Delta t\, v_i(x_i, y_i)^*$$

where (u_i, v_i) is the velocity of the ith sheet as determined from (3.17) and (3.18), and η_i is the random jump. Again, we have used Heun's method for the time integration. The value of this will be dicussed in the next section.

All that remains is to satisfy the boundary conditions at the wall. We can easily satisfy the requirement that vorticity not be allowed to diffuse through the boundary by reflecting any sheet attempts to cross. To satisfy the no-slip condition that $u = 0$ at $y = 0$, we create vorticity along the boundary as follows. At the beginning of each time step calculate the u component of the velocity along the wall at points spaced a distance h along the wall. If u is not zero at any point, create enough vortex sheets to provide a transition from the no-slip requirement to the value of u, and proceed with the algorithm using (3.19)–(3.20). Though both u and v will, by construction, be zero for each of these newly created sheets, the random walk term will diffuse them off the wall into the flow where they will join the other sheets.

D. *Matching of Interior and Boundary Layer Solutions*

To match the interior calculation to the boundary layer algorithm, we take the velocity component tangential to the solid walls produced by the vortex blobs as the free stream velocity seen at infinity by the boundary layer. This allows the interior calculation to determine the production of vorticity within the boundary layer. We transfer vorticity from the boundary layer to the interior by allowing those vortex sheets located a distance greater than δ (to be determined later) from the wall to become vortex blobs. Conservation of circulation arguments show that a vortex sheet of strength ξ should transform into a blob of strength ξh, where again h is the length of the sheet. Conversely, if a blob moves to a position less than δ from a wall, it becomes a sheet with strength ξ_{blob}/h. By taking δ large relative to the variance of the steps, it is unlikely that a blob will move outside the domain in one time step; if this does occur, we throw the element away.

We may summarize our algorithm for modeling the hydrodynamic part of the calculation as follows. Given at time $n\Delta t$ a collection of vortex blobs and sheets:

(1) Find $\bar{u} + \bar{u}_{\text{pot}}$ for each blob (3.9).

(2) Find the value of $\bar{u} + \bar{u}_{\text{pot}}$ tangential to the boundary, and use this as the free stream velocity to compute (u_i, v_i) for each sheet.

(3) Create vorticity as needed to satisfy the no-slip condition by adding vortex sheets on the boundary.

(4) Move sheets and blobs according to (3.19)–(3.20), with the stipulation that if a sheet moves into the interior, it becomes a blob and vice versa.

We have yet to discuss out choices for σ, the size of the core cutoff, and δ, the depth of the boundary layer. It has been shown, see [12], that $\sigma = h/\pi$ is an appropriate cutoff value. If we take $\delta = 2\sqrt{2\Delta t/R}$, this will yield a boundary layer of appropriate scale $O((R)^{-1/2})$ (see [20]), and the probability of any blob moving outside the boundary layer in one jump will be small. It is important to realize that δ represents a numerical boundary layer. It allows us to avoid the problem of vortex blobs too close to the wall, and provides a transition from sheets to blobs.

We found that the use of a second-order time integration scheme for the vortex sheets was not worth the effort for two reasons. First, the advection field within the boundary layer is essentially a one-dimensional flow in a direction parallel to the wall and thus poses no great problem for a first-order scheme. The main component driving the sheets away from the wall is the diffusion term. Second, the implementation of a second-order scheme is a very complicated procedure, since sheets may turn into blobs during the predictor step and thus must be treated differently.

One final comment: At first glance it might seem that our approximation is not valid in the corners, since the Prandtl boundary layer equations break down there. However, since the size of the boundary layer is small compared to the length of the sheets, and since the free stream velocity provided by the vortices approaches zero near a corner (due to boundary conditions), a sheet will diffuse into the main flow and become a blob before it is carried into a corner. Thus, in the neighborhood of a corner, we are in fact solving the Navier–Stokes equations.

E. *Results*

In the first numerical experiment, we chose to model the "spin-down" of a high Reynolds number flow in a square region. This is similar to the driven cavity problem studied in [4] and [23]. With sides of unit length and $R = 1000$, we placed a vortex blob in the center of the square with strength such that the tangential velocity midway along each wall was initially equal to unity. We chose $h = 0.1$, that is, the length of each sheet was $1/10$ and sheets were created along each wall at intervals 0.1 apart. The time step Δt was chosen to that $\Delta t \cdot U_\infty^{\max}/h < 1$, where $U_\infty^{\max}$ is the maximum tangential velocity to the wall generated by the vortices. A value of $\Delta t = 0.05$ was sufficient to ensure that no sheet was advected downstream a distance greater than its length during one time step. Finally, we chose a maximum amount $\xi_{\max} = 0.2$ of vorticity that any one sheet could carry; if more was needed to satisfy the no-slip condition, extra sheets of strength $\xi_{\max}$ were added. At the end of the calculation, there were about 400 blobs and 100 sheets per wall.

In Figs. 2a, b, c, d we have displayed the velocity field on a 30×30 grid placed in the flow, where the magnitude of the vector at each grid point denotes the relative speed of the flow there. The fluid slows, due to the development of small coun-

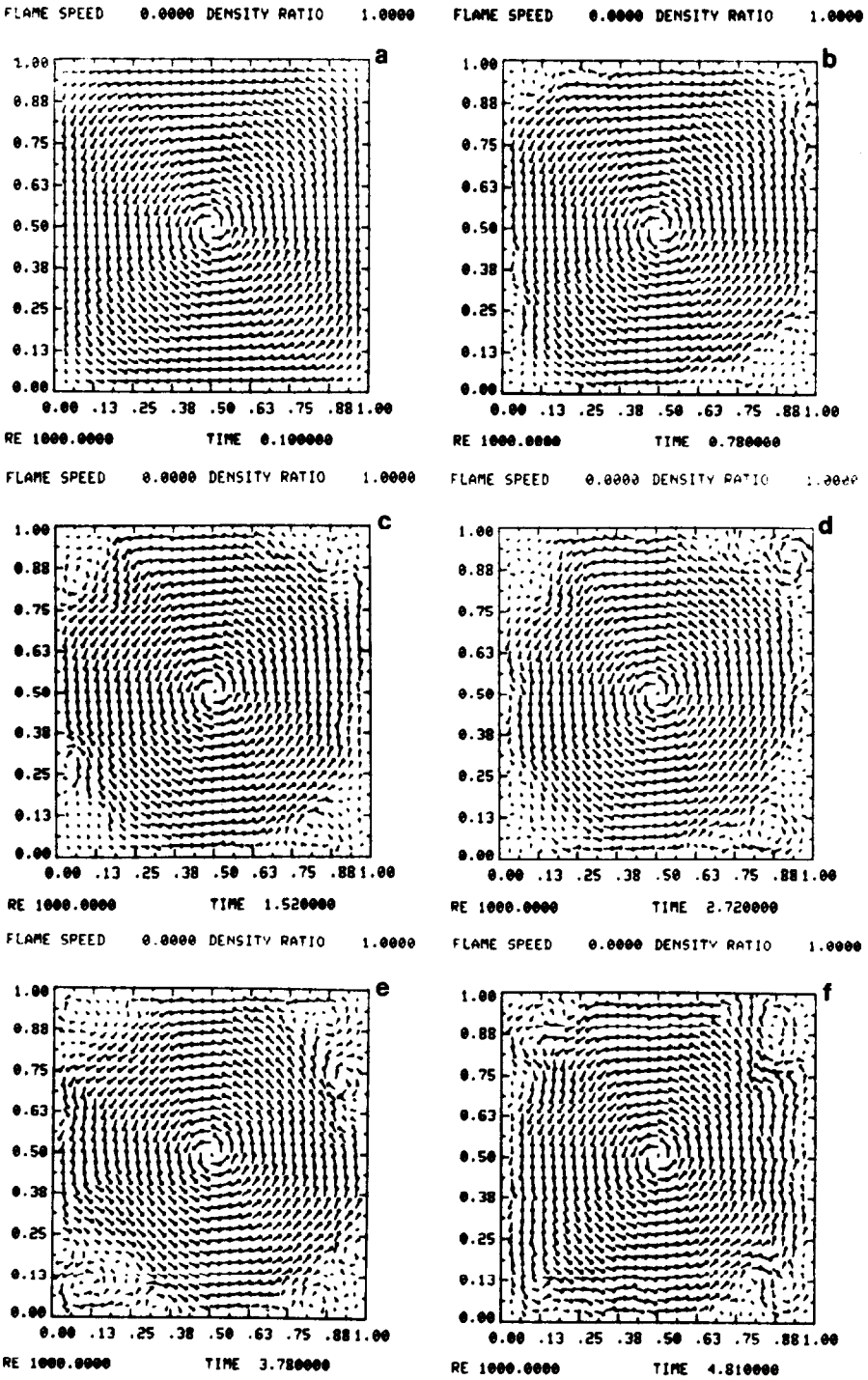
FLAME SPEED 0.0000 DENSITY RATIO 1.0000
a
1.00
0.88
0.75
0.63
0.50
0.38
0.25
0.13
0.00
0.00 .13 .25 .38 .50 .63 .75 .88 1.00
RE 1000.0000 TIME 0.100000
FLAME SPEED 0.0000 DENSITY RATIO 1.0000
b
RE 1000.0000 TIME 0.780000
FLAME SPEED 0.0000 DENSITY RATIO 1.0000
c
RE 1000.0000 TIME 1.520000
FLAME SPEED 0.0000 DENSITY RATIO
d
RE 1000.0000 TIME 2.720000
FLAME SPEED 0.0000 DENSITY RATIO 1.0000
e
RE 1000.0000 TIME 3.780000
FLAME SPEED 0.0000 DENSITY RATIO 1.0000
f
RE 1000.0000 TIME 4.810000

FIGURE 2

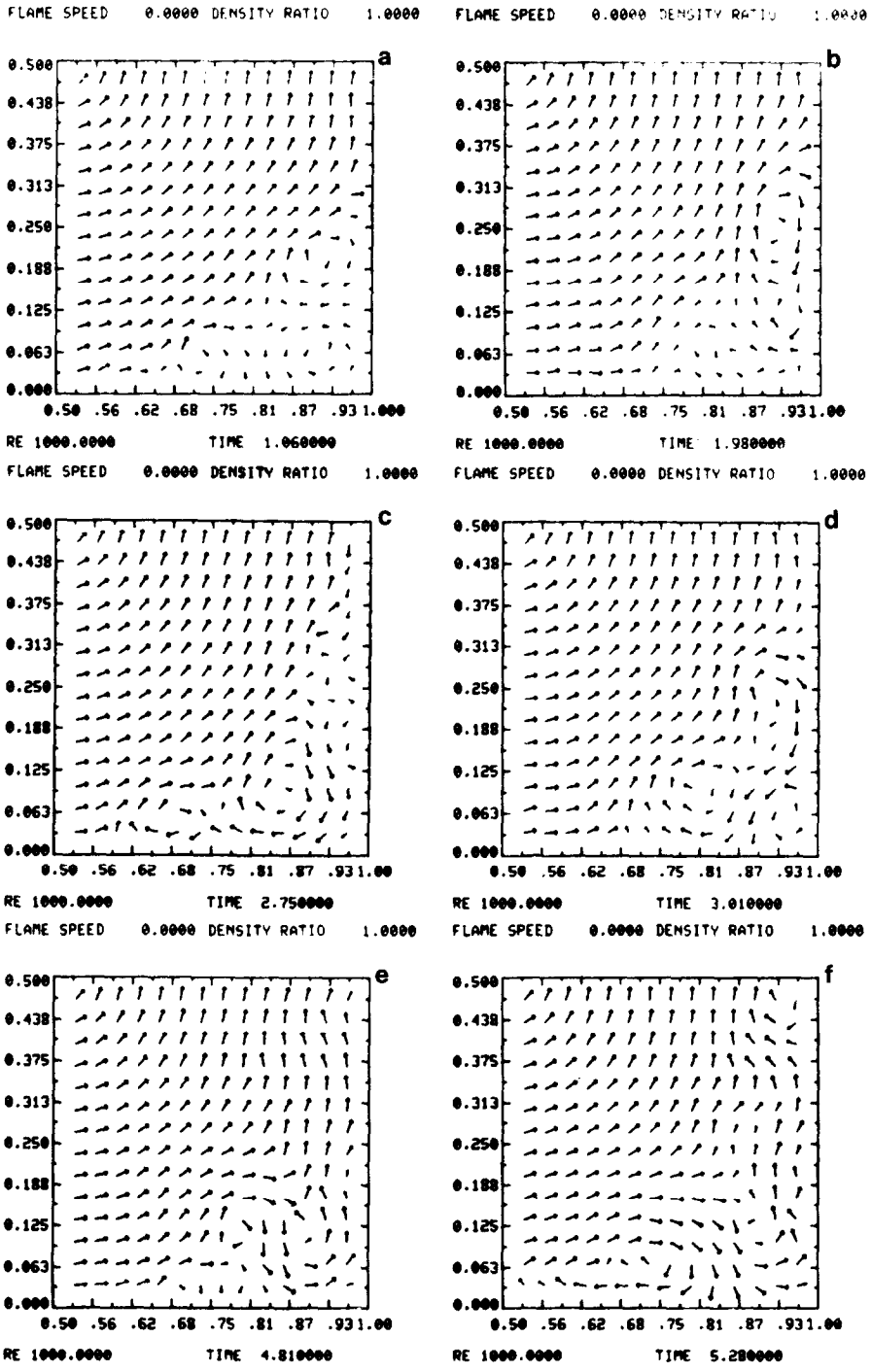
FLAME SPEED 0.0000 DENSITY RATIO 1.0000
a
0.500
0.438
0.375
0.313
0.250
0.188
0.125
0.063
0.000
0.50 .56 .62 .68 .75 .81 .87 .93 1.00
RE 1000.0000 TIME 1.060000
FLAME SPEED 0.0000 DENSITY RATIO 1.0000
b
RE 1000.0000 TIME 1.980000
FLAME SPEED 0.0000 DENSITY RATIO 1.0000
c
RE 1000.0000 TIME 2.750000
FLAME SPEED 0.0000 DENSITY RATIO 1.0000
d
RE 1000.0000 TIME 3.010000
FLAME SPEED 0.0000 DENSITY RATIO 1.0000
e
RE 1000.0000 TIME 4.810000
f
RE 1000.0000 TIME 5.280000

FIGURE 3

of concentrated vorticity. This process occurs in all four corners, symmetry is to be expected in neither the numerical model nor in real physical situations, since these structures grow and develop from small perturbations and are somewhat random. In Figs. 3a, b, c, d we focus on flow in the lower right corner. Qualitatively speaking, the small counterrotating eddies form a recirculation zone that grows until it reaches a certain maximum size or energy level. When this level is reached, the structure breaks into smaller eddies that diffuse downstream and is replaced by another set of coagulating structures.

Numerical experiments were performed for a range of time steps between $\Delta t = 0.005$ and $\Delta t = 0.05$, for maximum sheet strength $\xi_{\max}$ between 0.05 and 0.2, and for h (the length of a sheet) between 0.05 and 0.1. In the coarsest calculation (the one shown), the recirculation patterns in each corner were made up of about 100 vortices; in the finest calculation ($\xi_{\max} = 0.05$, $h = 0.05$), the recirculation zone in each corner was made up of about 700 vortices. Through these ranges of values, the above mechanism of recirculation growth and breakup remained essentially unchanged. The sizes of the recirculation zones and the length of time they lasted before breaking up were about the same. For a coarser calculation ($\xi_{\max} = 0.5$, $h = 0.2$), the situation was different; recirculation zones appeared and disappeared on the order of a few time steps. Clearly this was because not enough sheets were being created to adequately resolve the boundary layer; each sheet carried so much strength that when it become a blob it radically affected the flow. For this crude a calculation, numerical effects dominated.

One would like to be able to make quantitative measurements of the above mechanism of eddy formation and breakup. On a large scale, one can clearly see the formation and decay of the recirculation zones. However, it is not at all clear what parameters (size? energy? vorticity?) should be used to measure this process. As such, it is no easy task to describe the mechanism in a detailed way, and thus one is hesitant to make conclusions about small-scale effects. In a later paper, we shall address the issue of devising a technique to quantify such phenomena.

IV. Flame Propagation

It has been shown, see [21], that our equations of flame propagations (2.7)–(2.8) are analogous to hyperbolic systems of conservation laws. A front burning normal to itself can develop cusps, similar to shocks, where the front is no longer differentiable and the normal direction is not defined. This situation, plus an "entropy condition" implied by our model, poses serious and conceivably insurmountable difficulties for those numerical methods that attempt to use finite difference techniques to follow the motion of a front discretely parameterized by a set of marker particles. The technique we describe below, introduced in [9], avoids these difficulties and capitalizes on the geometric nature of flame propagation described in [21].

A. *Numerical Algorithm*

We again use the technique of operator splitting to break the motion of the flame into a burning step and an advection step. To describe the burning step, consider a simple closed curve γ such that all the particles inside γ are burnt and those outside are unburnt. At $t = 0$, we ignite all the particles on γ. Let $D(t)$ be the union of all disks of radius kt with centers on γ, together with the interior of γ (called D_γ). The position of the flame front at time t is given by the boundary of $D(t)$; this is, of course, a construction based on Huyghens' principle. An alternate way to produce $D(t)$ is to let $D^\theta(t)$ be the translation of the original region D_γ a distance kt in the direction $(\cos\theta, \sin\theta)$. The union of all such possible translations as θ ranges from 0 to 2π produces the expanded region $D(t)$. Our numerical algorithm is an approximation of this construction.

Assume, for the moment, that we possess an algorithm that will translate the given region D_γ in a given direction at a given speed (we shall discuss such an algorithm shortly) and consider the eight angles $\theta_l = (l-1)\,\pi/4$, $l = 1,\ldots, 8$. If we form the eight regions $D_\gamma^{\theta_l}(\Delta t)$, each one being the translation of the original region D_γ a distance $k\,\Delta t$ in the direction $(\cos\theta_l, \sin\theta_l)$, then the union of these regions together with the D_γ will approximate the burnt region at time Δt.

The algorithm used in [9] to translate D_γ in the eight directions is the Simple Line Interface Calculation (SLIC) method [17]. We impose a square grid i, j on the combustion domain, and assign a number f_{ij}, $0 \leqslant f_{ij} \leqslant 1$, to each cell, corresponding to the fraction of fluid within that cell that is burnt. The algorithm moves the burnt region by drawing in each cell for which $0 < f_{ij} < 1$ an interface which represents the boundary between the burnt and unburnt fluid. The orientation of the interface depends on the value of f_{ij} in both the cell and its neighbors. The burnt fluid is then transported in the given direction, and a new set of f_{ij} are created, approximating the burnt region translated a distance $k\,\Delta t$.

Using this algorithm, we may move the front in a direction normal to itself to model burning. At time $t = n\,\Delta t$, we have an array of cell fractions $f_{ij}(n)$. Let $f_{ij}^{\theta_l}(n)$ be the array of cell fractions obtained from moving the burnt region at time t in the direction θ_l. Let $f_{ij}^{\theta_0}(n) = f_{ij}(n)$. Then the burnt region at time $(n+1)\,\Delta t$ will be approximated by

$$f_{ij}(n+1) = \max_{0 \leqslant l \leqslant 8} f_{ij}^{\theta_l}(n). \tag{4.1}$$

This advances the front in a direction normal to itself a distance $k\,\Delta t$.

To update the position of the flame relative to the advection term, we need only transport the new array f_{ij}, using SLIC, in the direction prescribed by the hydrodynamic calculation.

We have made changes in the flame propagation algorithm used in [10]. To translate the burnt region in a direction not parallel to the x or y axis, SLIC decomposes the motion into a translation in the x direction (of the appropriate length), followed by a translation in the y direction. Numerical experiments on simple examples show that this does not necessarily give the same result as "sweeping" in the y direction

first, followed by x, because of the way in which interfaces are constructed. One possible solution, of alternating the order of the sweeps, was found to be ineffective. Instead, we perform both combinations and take as our new volume fraction in each cell the maximum of the two results. This preserves symmetry by removing a bias towards the x sweep present in earlier calculations.

A further improvement was motivated by the observation that the flame front tended to spread out over many cells whenever vortices came very close to the boundary between burnt and unburnt fluid, creating a "band" several squares wide of partially burnt cells around the front. This was due to the fact that the velocity field produced by the hydrodynamic calculation was not numerically divergence-free on the grid used to advect the flame. Thus, the grid representation of the velocity field due to vortices near the flame front violated conservation of mass. The solution was to use the technique described in [6] to create a grid divergence-free field from the original one. Other techniques, such as evaluating the velocity field directly at the edge of the flame, will be investigated in later work.

B. *Results*

We modeled combustion within our closed square. We took a 60×60 grid of flame cells, and let $k = 0.2$, where k is the burning speed in (2.7)–(2.8).

In our first experiment, we assumed that the fluid was inviscid and thus omitted the random motion and ignored the production of vorticity by the no-slip condition; only the normal boundary condition was met. With a single vortex blob in the center representing a swirling, steady, inviscid flow, we ignited the cell located halfway up the left side (i.e., set its volume fraction equal to unity). We enforced continuous ignition, that is, if unburnt fluid was swept into this cell, it too was ignited. In Fig. 4, we show the results of the experiment. For the purposes of display, we have shaded in those cells for which $f_{ij} > 0.2$. As the flame burns in a direction normal to itself into the vessel, it is advected by the flow; the combined motion causes the flame to spiral in towards the vortex blob. In Fig. 4c, we see that the flame has wrapped around the center several times. In Fig. 4d, the unburnt region between the layers of the spiral is beginning to burn. This illustrates a central feature of our method; simply because two partially burnt cells are close doesn't necessarily mean that the cells between them are burnt. We cannot overemphasize how much trouble this raises for those tracking algorithms based on connected marker particles. To advance the front due to burning, such techniques must use neighboring markers along the flame front to determine the normal direction. In the situation presented on Fig. 4e, it is not clear how the markers are joined. Thus, at each time step such a technique must "decide" how and which markers are connected, and eliminate those no longer on the boundary of the flame. This problem is avoided by this flame propagation algorithm.

As a check of the accuracy of the flame algorithm, we performed the following calculation. After 2.255 seconds (Fig. 4e), the distance from the leading tip of the flame to the center of the square is ≈ 0.07. Since the flame is burning in towards the center at a constant rate (as well as being advected by swirling flow, of course), the

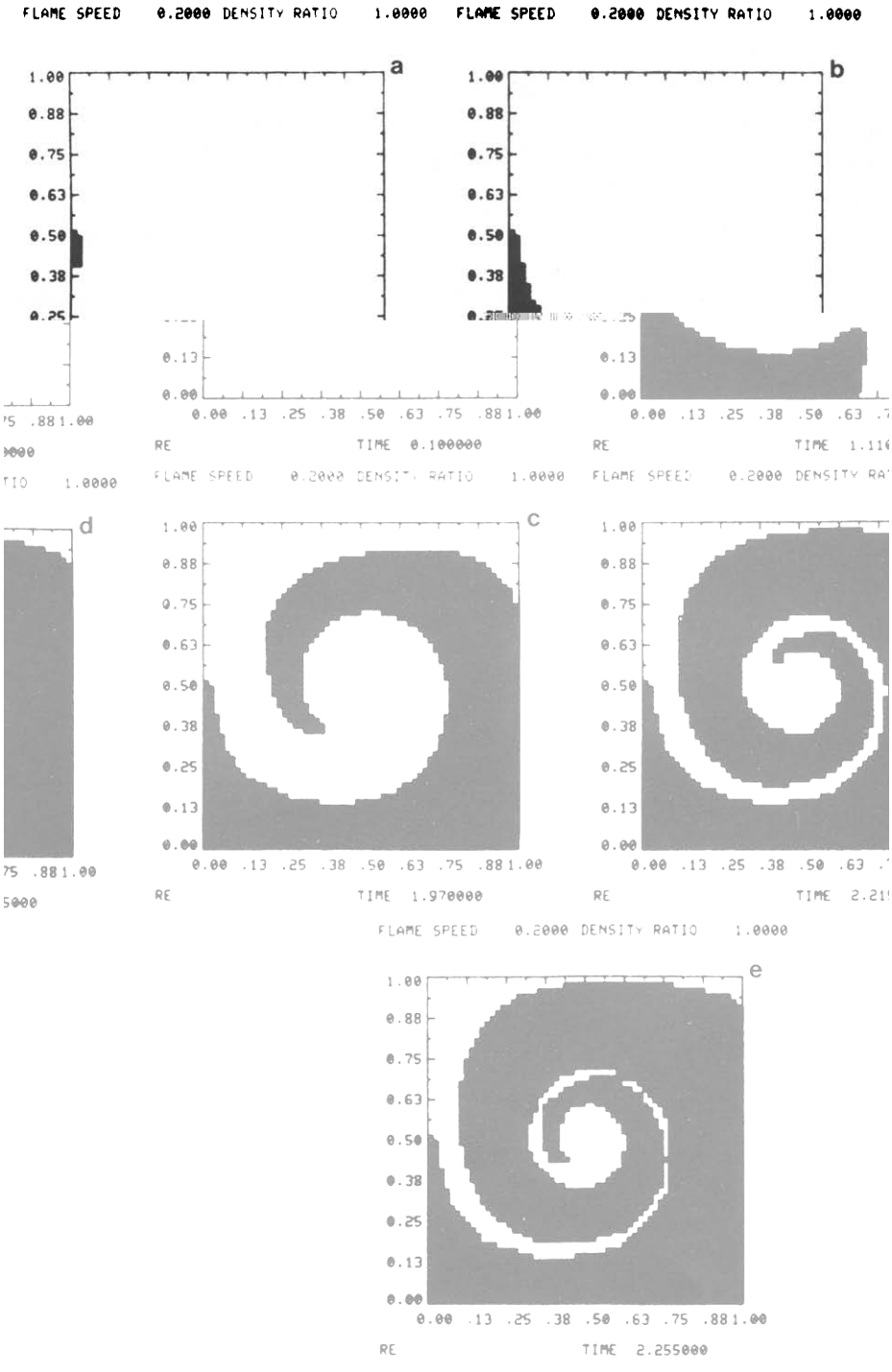
FLAME SPEED 0.2000 DENSITY RATIO 1.0000
FLAME SPEED 0.2000 DENSITY RATIO 1.0000
a
b
c
d
e
1.00
0.88
0.75
0.63
0.50
0.38
0.25
0.13
0.00
0.00 .13 .25 .38 .50 .63 .75 .88 1.00
RE
TIME 0.100000
TIME 1.970000
TIME 2.255000

FIGURE 4

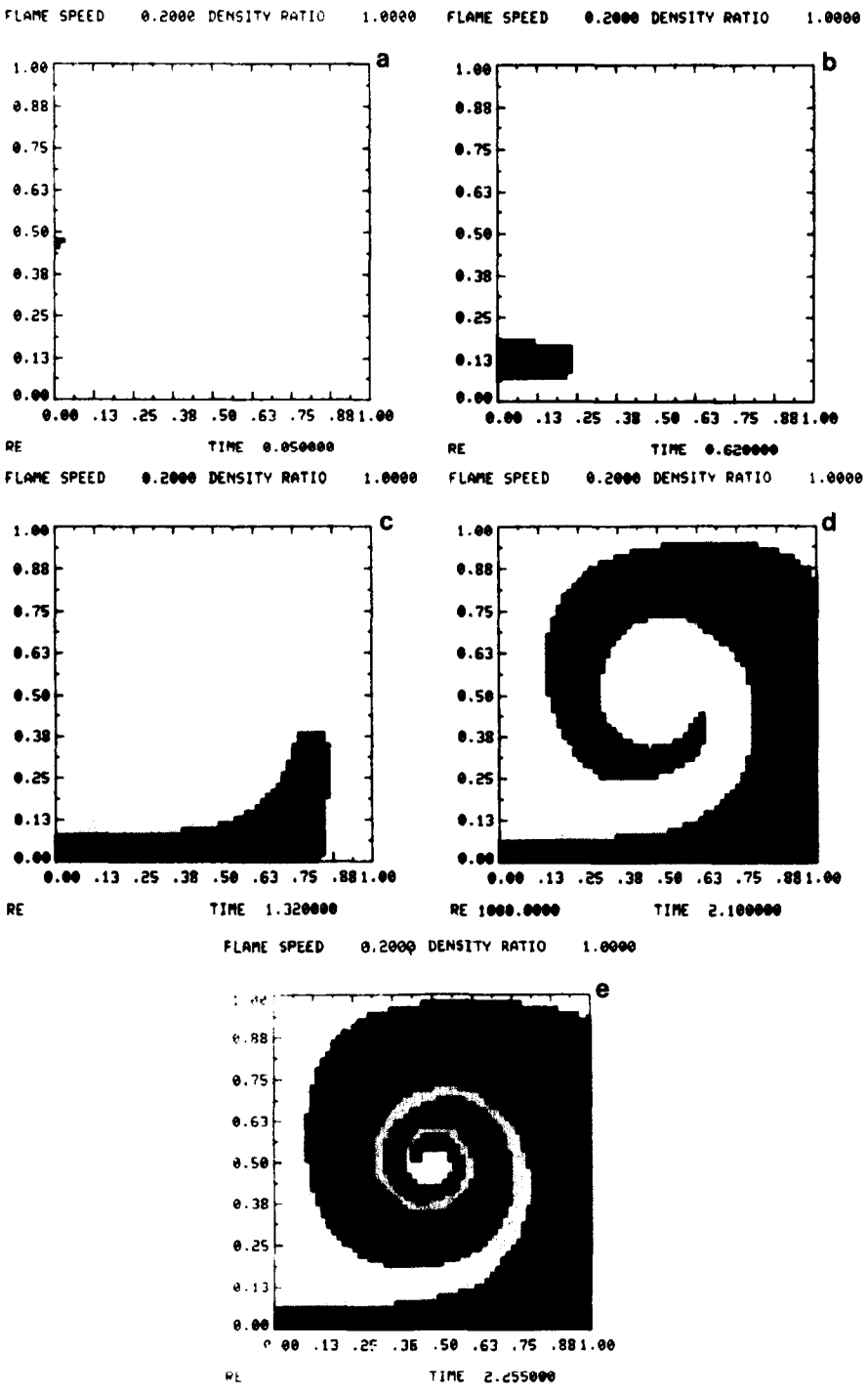
FLAME SPEED 0.2000 DENSITY RATIO 1.0000
a
1.00
0.88
0.75
0.63
0.50
0.38
0.25
0.13
0.00
0.00 .13 .25 .38 .50 .63 .75 .88 1.00
RE
TIME 0.050000
FLAME SPEED 0.2000 DENSITY RATIO 1.0000
b
RE
TIME 0.620000
FLAME SPEED 0.2000 DENSITY RATIO 1.0000
c
RE
TIME 1.320000
FLAME SPEED 0.2000 DENSITY RATIO 1.0000
d
RE 1000.0000
TIME 2.100000
FLAME SPEED 0.2000 DENSITY RATIO 1.0000
e
TIME 2.255000

FIGURE 5

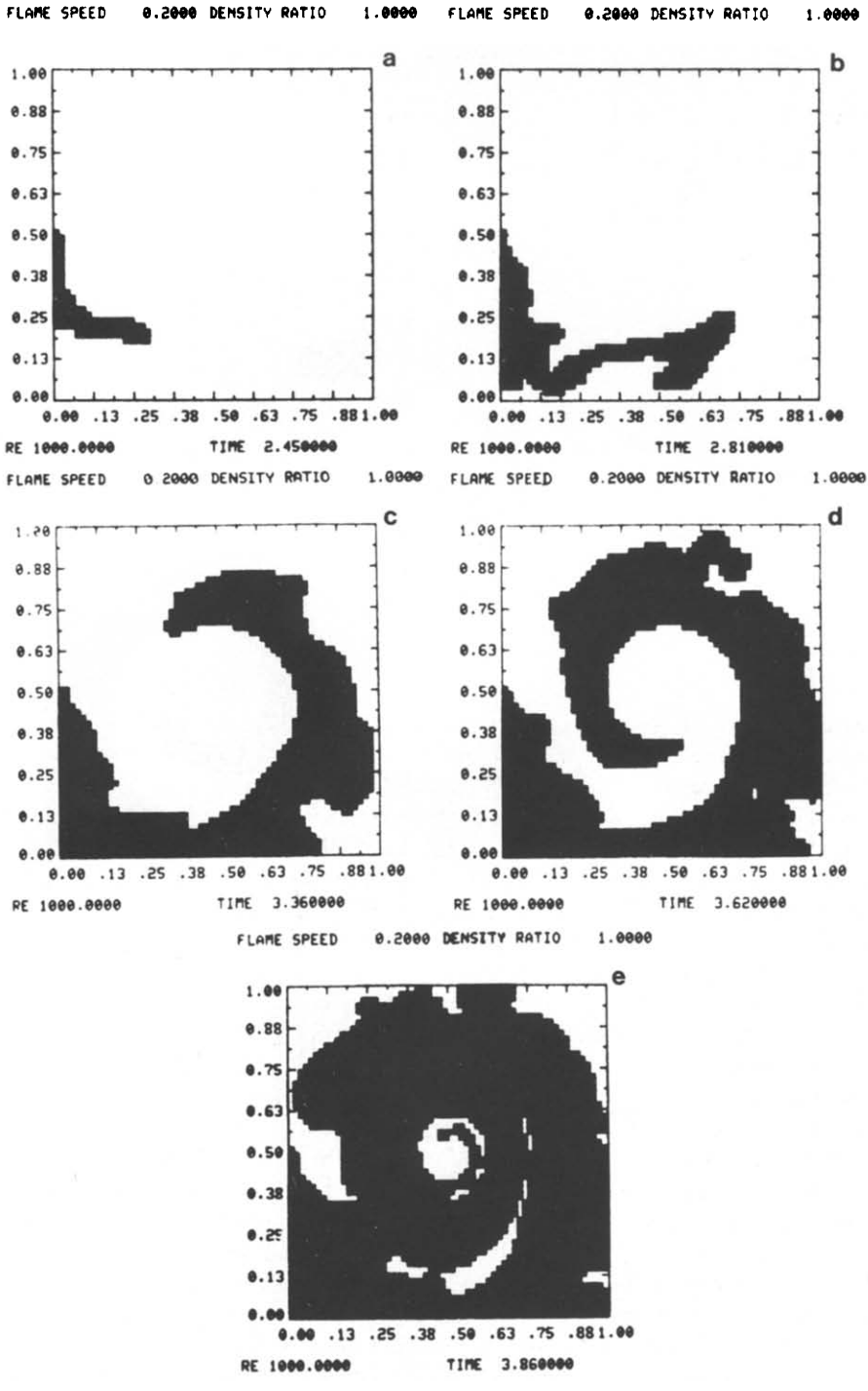
FLAME SPEED 0.2000 DENSITY RATIO 1.0000
a
1.00
0.88
0.75
0.63
0.50
0.38
0.25
0.13
0.00
0.00 .13 .25 .38 .50 .63 .75 .88 1.00
RE 1000.0000 TIME 2.450000
FLAME SPEED 0.2000 DENSITY RATIO 1.0000
b
1.00
0.88
0.75
0.63
0.50
0.38
0.25
0.13
0.00
0.00 .13 .25 .38 .50 .63 .75 .88 1.00
RE 1000.0000 TIME 2.810000
FLAME SPEED 0.2000 DENSITY RATIO 1.0000
c
1.00
0.88
0.75
0.63
0.50
0.38
0.25
0.13
0.00
0.00 .13 .25 .38 .50 .63 .75 .88 1.00
RE 1000.0000 TIME 3.360000
FLAME SPEED 0.2000 DENSITY RATIO 1.0000
d
1.00
0.88
0.75
0.63
0.50
0.38
0.25
0.13
0.00
0.00 .13 .25 .38 .50 .63 .75 .88 1.00
RE 1000.0000 TIME 3.620000
FLAME SPEED 0.2000 DENSITY RATIO 1.0000
e
1.00
0.88
0.75
0.63
0.50
0.38
0.25
0.13
0.00
0.00 .13 .25 .38 .50 .63 .75 .88 1.00
RE 1000.0000 TIME 3.860000

FIGURE 6

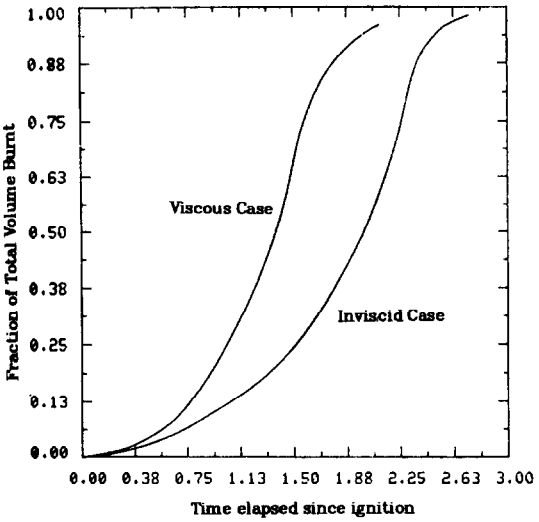

FIGURE 7

distance from the front tip to the center is given by $0.5 - kt$, where k is the flame speed and t is time. At $t = 2.255$ seconds, with $k = 0.2$ as in Fig. 4, the distance from the flame to the center should be $0.5 - (0.2)(2.255) \approx 0.05$.

We then repeated the experiment, choosing this time to ignite the fluid located in the ignition cell only once. Fluid swept into this cell at a later time was left unchanged. The results of this "sparked" ignition are shown in Fig. 5. The small patch of burning fluid (Fig. 5a) is carried into the lower left corner where the flow is slow enough so that burning dominates advection and the corner remains burnt (Fig. 5b). The flame spreads along the bottom wall, advected by the flow (Fig. 5c), and again spirals towards the center (Figs. 5d, e).

In both calculations, we chose an initial time step of $\Delta t = 0.05$. The increase in advection speed as the flame burned towards the center eventually led to a violation of the time step requirement stated earlier. We then chose a smaller time step and continued the calculation, refining the time step whenever needed. A final time step of $\Delta t = 0.01$ was sufficient to allow the flame to fill the entire volume.

In the final experiment, we ignited the viscous, swirling flow modeled in Section III. Here, we waited until $t = 2.0$ second before ignition so that back flow in the corners would have time to develop. The flame moves down the left side (Fig. 6a) where it encounters the first recirculation zone and is forced over the top of the large eddy located in the lower left corner. It is then pushed down against the bottom wall, where part of it is carried by the recirculation zone backwards into the left corner (Fig. 6b). As the front reaches the lower right corner (Fig. 6c), the same phenomenon occurs as the eddy first pushes the flame away and then grabs it from behind.

Because of the formation of time-dependent recirculation zones created by viscous effects, the flame front becomes jagged and wrinkled (Fig. 6d). This is in contrast to the smooth flame front presented in the inviscid case (Fig. 4d). In Fig. 7 we have plotted the fraction of the total volume that is burnt against the amount of time elapsed since ignition. The effect of viscosity can clearly be seen; after starting off close together, the top curve (viscous case) splits away from the bottom curve (inviscid case) as the viscous flame passes through eddies created by the no-slip condition on the walls. These eddies stretch and distort the boundary between the burnt and unburnt fluids, providing a longer flame front and hence more contact with unburnt fluid available for combustion. Around 1.5 seconds after ignition is the

V. Effects of Exothermicity

In this section, we would like to allow for density differences between the burnt and unburnt gas and thereby include the effects of volume expansion along the flame front. As explained earlier, our model does not allow us to consider these effects inside a closed vessel, thus the numerical technique described below will only be used for open vessel calculations. However, in a later paper [22], we show that this same technique can be modified to handle more sophisticated models of combustion for closed vessels in which pressure changes are allowed.

The effect of volume expansion along the flame front is reflected in the momentum equation

$$\frac{D\vec{u}}{Dt} = \frac{1}{R}\nabla^2\vec{u} - \frac{\nabla\vec{P}}{\rho} \tag{5.1}$$

and the continuity equation

$$\frac{1}{\rho}\frac{D\rho}{Dt} + (\nabla \cdot \vec{u}) = 0. \tag{5.2}$$

Since ρ is not constant across the front, the pressure term $\nabla\vec{P}/\rho$ no longer vanishes when we take the curl of (5.1). Thus, vorticity is produced along the flame front by the jump in density. In this model, we shall ignore this production term and assume that Eq. (3.1) holds throughout the domain; we focus solely on the effects of the density jump on the continuity equation.

A. *Numerical Algorithm*

To approximate Eq. (5.2), we need to express the change in volume along the front in terms of our flame algorithm. For any given cell, let M^n be the total mass of the

fluid in that cell at time $n\,\Delta t$, and let V_u^n and V_b^n be the volumes of the unburnt and burnt fluid, respectively. Then,

$$M^n = \rho_b V_b^n + \rho_u V_u^n$$
$$M^{n+1} = \rho_b V_b^{n+1} + \rho_u V_u^{n+1}.$$

Let $\Delta f_{ij}^{\text{burn}}$ be the change in the volume fraction produced by the propagation of the flame due to burning (the combustion step). Since f_{ij} measures the fraction (between 0 and 1) of burnt fluid in the cell, then

$$V_b^{n+1} - V_b^n = h^2\,\Delta f_{ij}^{\text{burn}}$$
$$V_u^{n+1} - V_u^n = -h^2\,\Delta f_{ij}^{\text{burn}}$$

where h^2 is the area of the cell. If we let ΔM be the change in the total mass of the fluid contained in the cell, then

$$\Delta M = M^{n+1} - M^n = h^2\,\Delta f_{ij}^{\text{burn}}(\rho_b - \rho_u).$$

Since $\Delta\rho$, the change in density, is given by $\Delta M/h^2$, we may approximate $(1/\rho)$ $(D\rho/Dt)$ by

$$\frac{1}{\rho}\frac{D\rho}{Dt} \approx \left[\frac{1}{(\rho_u+\rho_b)/2}\right]\left[\frac{\Delta f_{ij}^{\text{burn}}}{\Delta t}(\rho_u - \rho_b)\right] = 2\left\{\frac{\rho_u - \rho_b}{\rho_u + \rho_b}\right\}\frac{\Delta f_{ij}^{\text{burn}}}{\Delta t}. \tag{5.3}$$

If we use a staggered grid for the velocities (see Fig. 8), then we may approximate (5.2) by

$$\frac{u_l - u_r + v_t - v_b}{h} = 2\left\{\frac{\rho_u - \rho_b}{\rho_u + \rho_b}\right\}\frac{\Delta f_{ij}^{\text{burn}}}{\Delta t} \tag{5.4}$$

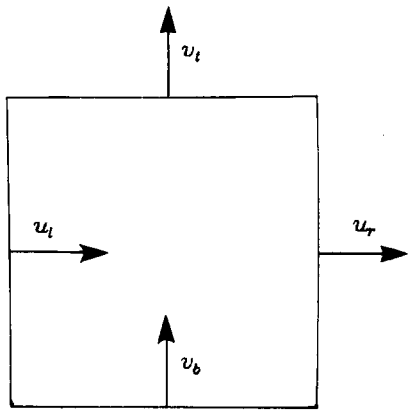

FIGURE 8

where $u_l(u_r)$ is the velocity normal to the left (right) side, and $v_t(v_b)$ is the velocity normal to the top (bottom) side. As a check, we note that if the front is propagating parallel to either the x or y axis, then $\Delta f_{ij}^{\text{burn}}/\Delta t = k/h$, where k is the propagation speed, and (5.4) reduces to (2.4).

The rest of this section is devoted to a discussion of how to find the exothermic velocity field accurately. In [10], volume source blobs of strength corresponding to the amount of volume produced at each time step were placed in the center of each cell for which $\Delta f_{ij}^{\text{burn}} > 0$. A potential flow was added to the velocity field induced by these sources to satisfy boundary conditions. One difficulty results from the placement of the source at the center of a cell undergoing combustion, regardless of the position of the flame in that cell; this causes an inaccurate calculation of the exothermic velocity at the front of the flame and accentuates the development of the "thick" flame front discussed earlier. We describe below a technique that avoids this problem by using information contained in SLIC to determine the exact location of the front as seen by our flame propagation algorithm. By placing sources of volume along the front, and then extrapolating onto the grid used by SLIC, we may use a fast Poisson solver to determine the exothermic velocity field.

To model the propagation of the flame in a direction normal to itself, our flame algorithm considers the effect of sweeping into a given cell the burnt fluid in each of its neighbors. The maximum of all these contributions is chosen as the new value for f_{ij}. Since only one of these neighbors is allowed to determine the new value, this means that the front can be viewed as propagating into the given cell from a particular direction. Thus, our technique for placing volume sources is as follows: for each cell we keep track of which neighbor was the "contributor," and which of the possible shapes used by SLIC were involved in the horizontal and vertical sweeps of the "contributor" into the given cell. From these shapes, we place the volume source along the front edge of the flame as it sweeps into the cell. Although the full catalogue of all possible shapes and the possible ways they can influence the cell

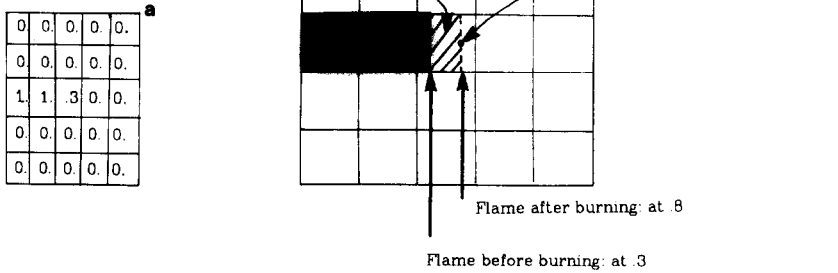

FIGURE 9

represents a formidable programming task, the computing time involved is minimal since the proper configuration can easily be found and evaluated.

As a simple example, suppose the array of volume fractions before the burning step is as in Fig. 9a. With $k = h = 1$ and $\Delta t = 0.5$, the contributor to the center square will be the cell directly on its left, and the shape of the flame as constructed by SLIC is the vertical front shown in Fig. 9b. The vertical front burns to the right a distance 0.5 and the volume fraction increases from 0.3 to 0.8; thus we place a volume source of strength $\Delta f_{ij}^{\text{burn}} = 0.5$ on the edge of the newly placed front. If instead we use a time step $\Delta t = 1$, the placement changes slightly. Here, the flame moves out of the center

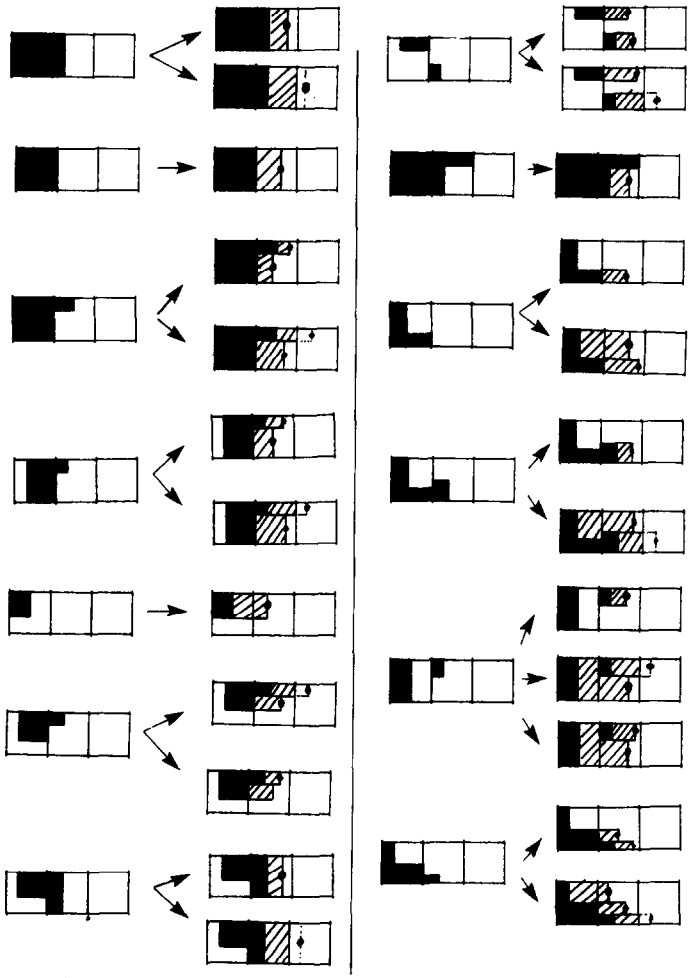

FIGURE 10

cell and into the cell on the right a distance 0.3; it is there that we must place the volume source of strenght 0.7. (Note that the center cell acts as a contributor when we update the cell on its right, thus providing the "missing" 0.3.)

When the contributor cell is diagonal to the cell being evaluated, we use the last sweep (either vertical of horizontal) to determine the placement of volume sources. In some cases there may be more than one volume source per cell. A catalogue of basic shapes (ignoring symmetries) and accompanying location for volume sources is given in Fig. 10. Here, we have assumed the left cell acts as the contributor for the cell in the center, and have shown the placement of volume sources for burning into the center cell. Those volume sources extending into the right cell are placed when that cell is evaluated.

Given the location and strengths of these volume sources, they form the right-hand side of a Poisson's equation for the exothermic velocity; that is, we want to find a function φ_{vol} such that

$$\nabla^2 \varphi_{\text{vol}} = 2 \left\{ \frac{\rho_u - \rho_b}{\rho_u + \rho_b} \right\} \frac{\Delta f_{ij}^{\text{burn}}}{\Delta t}.$$

To use a fast Poisson solver on the grid provided by the flame cells, we need to find the proper discrete right-hand side corresponding to our volume sources. In the current calculation, we use the easiest possible method and simply linearly extrapolate the sources onto the grid. Admittedly, this may sacrifice some of the accuracy obtained by knowing the location of the flame, however, for a flat flame burning down a tube, this technique produces the exact constant flame speed (burning + advection), regardless of grid size. Such techniques as particle in cell, etc., may provide more effective ways of using the available information to accurately construct the appropriate right-hand side; we shall not explore their use here. The boundary conditions for this velocity field $(u, v) = \nabla \varphi_{\text{vol}}$ require that the normal derivative of φ_{vol} along solid walls be zero, and that

$$\int_{\text{open sides}} (\nabla \varphi_{\text{vol}} \cdot \vec{n}) = 2 \left\{ \frac{\rho_u - \rho_b}{\rho_u + \rho_b} \right\} h^2 \sum_{i,j} \Delta f_{ij}^{\text{burn}} \tag{5.5}$$

The above is just an expression of the Neumann compatibility condition that volume produced within the interior must be allowed to leave through the exit. This velocity field, together with the hydrodynamic component, constitutes the advection field for both the flame and the vorticity calculation.

B. *Results*

We modeled turbulent flow in a channel to analyze the effect of exothermicity and viscosity on the speed and shape of the burning flame. The combustion domain was a rectangle, lying along the x axis, with sides of length 5. and height 1. Fluid entered the channel with uniform speed ($U_{\text{entrance}} = 5.$) through a slit at the left end. At the exit, we imposed Poiseuille flow. (See Fig. 11.) We used a 400×80 grid and chose a

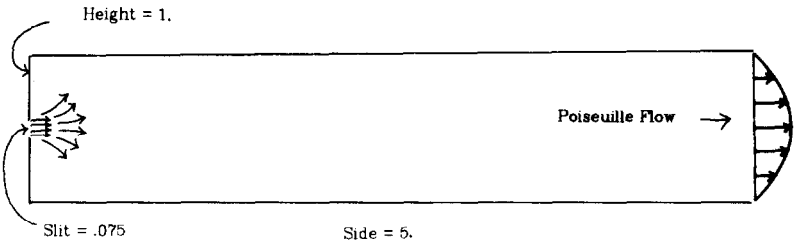

FIGURE 11

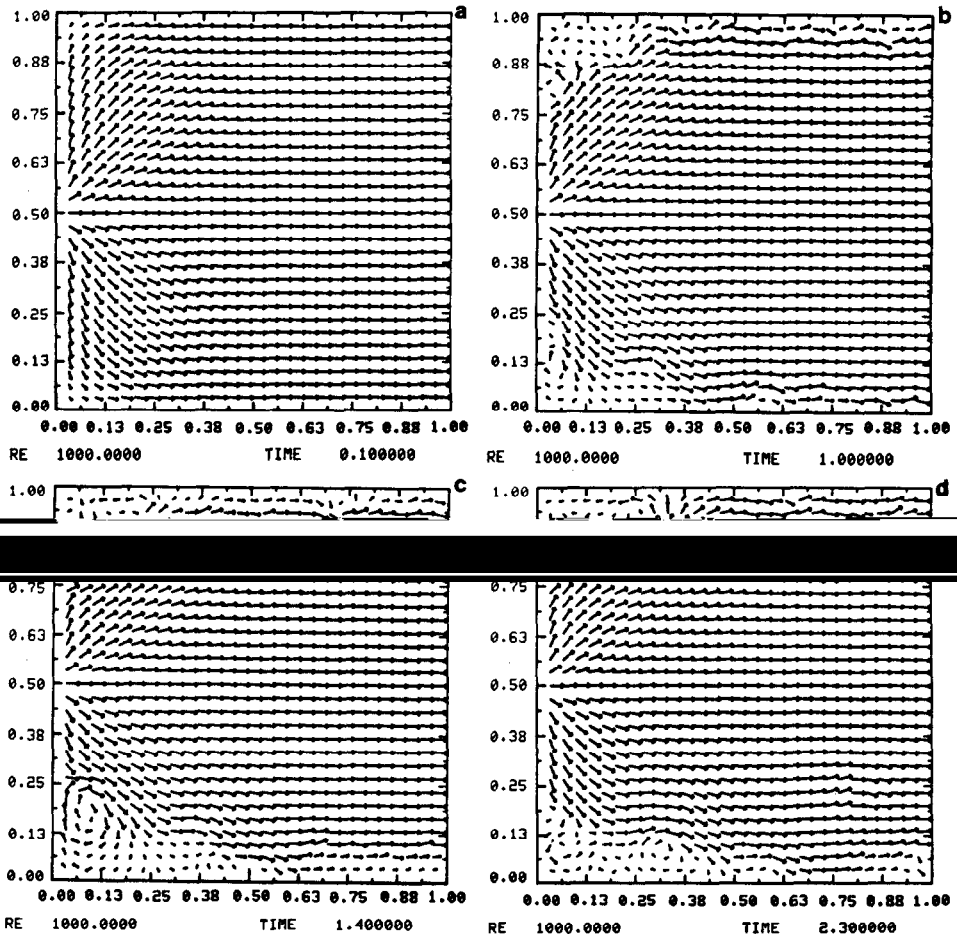

FIGURE 12

time step $\Delta t_{\text{vor}} = 0.1$ for the vortices and $\Delta t_{\text{flame}} = 0.01$ for the flame. As in Section III, we varied Δt_{vor}, $\xi_{\max}$, and h within the aforementioned range with little qualitative variation in results. Although a more physically realistic problem might be to include the effects of entrance vorticity on the flow, we wanted a simple configuration where we could isolate the interaction between vorticity generated in the corners, exothermic effects, and flame motion.

In the first experiment, we show the effect of viscosity (Re = 1000) on the flow. In Figs. 12a, b, c, d we have shown the velocity vectors for the first fifth of the channel. After the flow enters through the slit (Fig. 12a), small counterrotating eddies build in the corners (Fig. 12b). These eddies grow larger (Fig. 12c) until they break off and

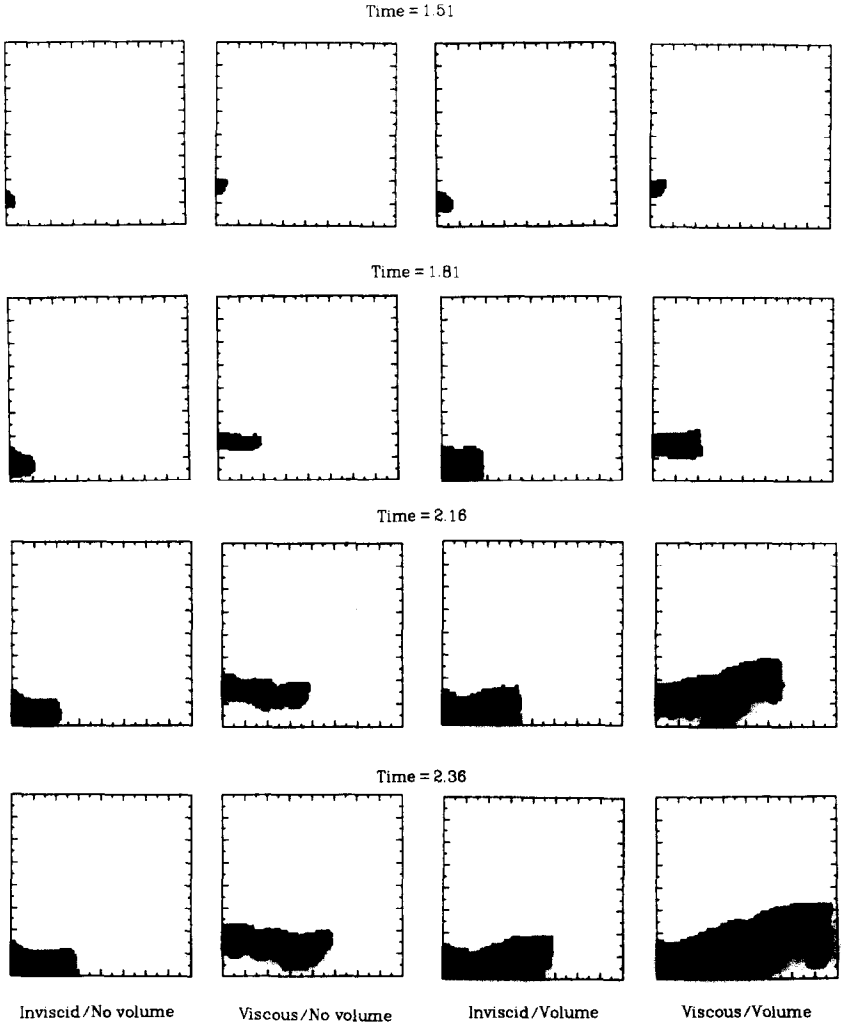

FIGURE 13

diffuse downstream (Fig. 12d). Long-time calculations show a continual process of eddy formation, growth, and diffusion.

In the next set of experiments (Fig. 13), we detail the effects of volume expansion and viscosity on the flame's motion. We ignited the fluid at the point (0,3/16). We chose this point so that we could study the interaction between the flame and the recirculation zones in the lower left corner; of course, ignition at a different point would produce different results. In the first run, we assumed an inviscid flow with $\rho_u = \rho_b = 1$, thus there was no volume expansion along the front (Inviscid/No volume). In the second run, we let $\mathrm{Re} = 1000$ and $\rho_u = \rho_b = 1$ (Viscous/No volume). In the third run, we assumed inviscid flow with $\rho_u = 1$ and $\rho_b = 0.2$ (Inviscid/Volume), thus there was a ratio of unburnt to burnt of $\rho_u/\rho_b = 5$. In the last experiment, we combined both effects (Viscous/Volume). Results were checked by varying the grid size between 300×60 and 500×100 with little variation in the results.

The results can be analyzed as follows. Without volume sources or viscosity, the flame moves smoothly through the flow. The addition of viscosity (Viscous/No volume) causes the flame to be caught up in recirculation zones in the corners and swept away from the boundary. The bottom side of the front becomes jagged as it is carried downstream by the eddies. The front tip of the flame is thrown forward by the recirculation eddies, and the front wrinkles in response to local variations in the flow introduced by diffusing vorticity.

When viscosity is ignored and the fluid is allowed to expand upon burning (Inviscid/Volume), the results are quite different. The flame can easily burn up to the walls, and moves down the channel more quickly due to the advection field produced by volume expansion. Note that the front is smooth, reflecting the lack of turbulent

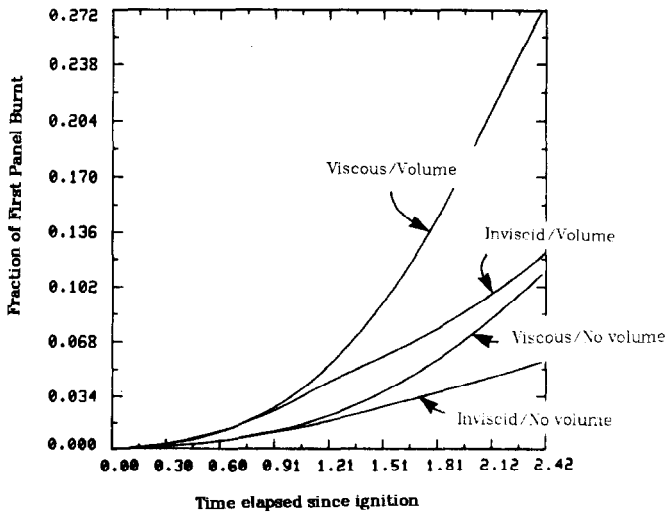

FIGURE 14

eddies. Finally, in the case where both density variations and viscosity are included (Viscous/Volume), the maximum amount of combustion occurs. The advection field associated with volume expansion carries the front into faster moving parts of the flow, and while viscosity keeps the flame away from the walls, it throws the tip of the flame downstream and wrinkles the front, increasing the amount of surface area available for combustion. In Fig. 14, we plot the fraction of burnt fluid in the first fifth of the channel against the time elapsed since ignition. To summarize, we may say that (a) exothermicity increases the rate of combustion and (b) while viscosity inhibits combustion near the walls, it increases burning in the interior.

ACKNOWLEDGMENTS

I would like to thank Alexandre Chorin and Ole Hald for their useful suggestions and encouragement. Calculations were performed on a Vax 780 at the Lawrence Berkeley Laboratory.

REFERENCES

1. W. T. ASHURST, "Proceedings, 1st Symposium on Turbulent Shear Flows" (Durst *et al.*, Eds.), pp. 402–413, Springer–Verlag, Berlin/New York, 1979.
2. J. T. BEALE AND A. MAJDA, *Math. Comp.* **39** (1982), 1.
3. K. N. C. BRAY, Turbulent flows with premixed reactants, *in* "Turbulent Teacting Flows" (P. A. Libby and F. A. Williams, Eds.), Chapter 5, Springer–Verlag, New York/Berlin, 1980.
4. O. D. BURGRAFF, *J. Fluid Mech.* **24** (1966).
5. A. CHEER, *SIAM J. Sci. Stat. Comput.* **4** (1983), 4.
6. A. J. CHORIN, *Math. Comp.* **22** (1968), 745.
7. A. J. CHORIN, *J. Fluid Mech.* **57** (1973), 785.
8. A. J. CHORIN, *J. Comp. Phys.* **27** (1978), 428.
9. A. J. CHORIN, *J. Comp. Phys.* **35** (1980), 1.
10. A. F. GHONIEM, A. J. CHORIN, AND A. K. OPPENHEIM, *Philos. Trans. Roy. Soc. London Ser. A* **304** (1982), 303.
11. O. HALD AND V. DEL PRETE, *Math. Comp.* **32** (1978), 791.
12. O. HALD, *SIAM J. Numer. Anal.* **16** (1979), 726.
13. L. D. LANDAU AND E. M. LIFSHITZ, "Fluid Mechanics," Pergamon, New York, 1975.
14. A. LEONARD, *J. Comput. Phys.* **37** (1980), 289–335.
15. P. A. LIBBY AND F. A. WILLIAMS, Fundamental aspects, *in* "Turbulent Reacting Flows" (P. A. Libby and F. A. Williams, Eds.), Chapter 1, Springer–Verlag, New York/Berlin, 1980.
16. M. F. MCCRACKEN AND C. S. PESKIN, *J. Comput. Phys.* **35** (1980), 183–205.
17. W. NOH AND P. WOODWARD, "Proceedings, 5th Int. Conf. Num. Meth. Fluid Mechanics," Springer–Verlag, Berlin/New York, 1976.
18. W. C. REYNOLDS AND T. CECEBI,Calculation of turbulent flows, *in* "Turbulence" (P. Bradshaw, Ed.), Chapter 5, Springer–Verlag, Berlin/New York, 1978.
19. A. ROSHKO, *AIAA J.* **14** (1976), 10, 1349–1357.
20. H. SCHLICHTING, "Boundary Layer Theory," McGraw–Hill, New York, 1968.
21. J. A. SETHIAN, PhD Dissertation, Univ. of Cal., Berkeley, June 1982.
22. J. A. SETHIAN, "Numerical Simulation of Flame Propagation in a Closed Vessel," Fifth GAMM Conference on Numer. Meth. Fluid Mech., Rome, Italy, Oct. 1983.
23. A. I. SHESTAKOV, *J. Comput. Phys.* **31** (1979), 313.
24. P. SWARZTRAUBER AND R. SWEET, *NCAR Technical Report* **(TN/IA-109)** (1975).